J. Fluid Mech. (1995), *vol.* 305, *pp.* 347–371

Deep-water internal solitary waves

By ANDREW P. STAMP† AND MARCUS JACKA‡

Research School of Earth Sciences, The Australian National University, Canberra, ACT 0200, Australia

(Received 19 June 1992 and in revised form 21 June 1995)

An experimental investigation of mode-2 ('lump-like') solitary waves propagating on a thin interface between two deep layers of different densities is presented. Small- and large-amplitude waves behaved differently: small waves carried energy and momentum, whereas sufficiently large waves also carried mass. Weakly nonlinear theory anticipated the results for amplitudes $a/h \leqslant 0.5$ but did not provide even a qualitative description of the large-amplitude waves. In particular, the prediction that for waves to maintain permanent form their wavelength must decrease with increasing amplitude failed; instead the wavelength of large waves was observed to increase with increasing amplitude. Furthermore, whilst the waves were expected to emerge from interactions along their precollision trajectories, the large waves actually suffered a backward shift.

1. Introduction

Solitary waves have been of interest since Russell (1837) first observed a surface water wave of finite amplitude and permanent form. This classical solitary wave propagates on the free surface of a shallow homogeneous fluid of constant depth. The permanent form is due to a balance between dispersion and nonlinearity. Linear theory predicts that infinitesimal shallow-water waves have phase speeds $c_0(1 - \beta k^2)$ where $k = 2\pi/\lambda$ is the wavenumber, λ is the wavelength, c_0 is the long-wave ($k \ll 1$) speed and β is a positive constant. Hence long waves travel fastest. Conversely, if dispersion is ignored, then weakly nonlinear theory predicts phase speeds proportional to local vertical displacement. Hence long waves travel slowest. Thus a balance between dispersion and nonlinearity is possible for waves that are long compared to the fluid depth.

Recent interest has centred on solitary waves propagating in density-stratified fluids and it is now clear that dispersion and nonlinearity balance for waves that are long compared to either the total fluid depth or the depth over which the fluid density varies. These internal solitary waves can be excited by tropical sea-breeze fronts and mid-latitude cold fronts in the atmosphere (Christie 1992) and tidal flows over bottom topography in the ocean (Ostrovsky & Stepanyants 1989). Indeed, Maxworthy (1980) noted that "quite general and uncontrolled mixing events create internal solitary wave trains [and this] leads us to suspect that they should be excited under many circumstances in natural systems".

† Present address: University of Washington, School of Oceanography, Box 357940, Seattle, WA 98195, USA.

‡ Present address: Research School of Physical Sciences and Engineering, The Australian National University, Canberra, ACT 0200, Australia.

This study considers long deep-water internal solitary waves, that is, waves with wavelengths much smaller than the total fluid depth but much greater than the depth over which the fluid density varies. Such waves can, for example, propagate on a shallow fluid layer lying above or below a deep layer as well as on a thin pycnocline between two deep layers. A stunning example is the 'morning glory' roll cloud phenomenon observed on the atmospheric nocturnal inversion over northern Australia. These waves are often large enough to trap moisture and studies following the pioneering work of Christie, Muirhead & Hales (1978) indicate that they play an important role in the transfer of energy, mass and momentum as well as the generation and organization of turbulence in the lower atmosphere. Similar waves occur on the ocean thermocline excited by flow over a sill (Farmer & Smith 1980).

Small-amplitude deep-water waves have open streamlines and are well described by weakly nonlinear theory (Benjamin 1967; Davis & Acrivos 1967), whereas at large amplitudes the waves contain fluid trapped within closed streamlines and the approximate analytic results fail. To provide a quantitative understanding of waves with recirculating regions, Tung, Chan & Kubota (1982) computed numerical solutions to the fully nonlinear equation governing steady waves of arbitrary amplitude in inviscid fluids. Although deep-water waves were considered, the focus was on shallow-water waves, and thus the theoretical and experimental basis on which to interpret field observations of large-amplitude deep-water waves remains limited. This investigation uses laboratory experiments to extend our understanding of deep-water waves.

In each experiment a single large-amplitude wave was generated by displacing a paddle in a diffused interface between two deep layers of different densities. As the wave propagated, fluid was entrained into, mixed and then ejected from its recirculating region. Thus the waves not only transported fluid over large distances but also promoted localized mixing. As energy was dissipated, waves decreased in amplitude and eventually became too small to trap fluid. The wavelength of the large waves increased linearly with increasing amplitude and hence the wave profile only varied by a scaling factor. This self-scaling behaviour also occurs for solitary waves on the interface between two unbounded fluids of different densities (Pullin & Grimshaw 1988), and differs from the prediction of weakly nonlinear theory that for waves to maintain permanent form their wavelength must be smaller for larger amplitudes. However, whilst the wavelength–amplitude scaling was qualitatively different for small- and large-amplitude waves, the wavespeed was an insensitive measure of wave behaviour, increasing linearly with increasing amplitude for all waves. The rate of amplitude attenuation was also independent of amplitude, with dissipation occurring through viscous stresses, turbulent mixing and, possibly, wave radiation.

Experiments were also conducted to investigate wave–boundary and wave–wave interactions. At small amplitudes waves emerged from reflections against a solid vertical boundary unchanged and along their precollision trajectories, whereas at large amplitudes the reflected wave was smaller and slower than the incident wave and suffered a backward shift. The head-on collision between waves of equal amplitude was similar to a reflection, with the fluid trapped within each wave reversing direction and being transported away from the collision along the path by which it approached. For waves of different amplitudes this behaviour was modified by the exchange of fluid from the larger incident wave to the smaller incident wave such that the leftward and rightward propagating waves had the same amplitudes before and after the collision.

The structure of this paper is as follows. Section 2 outlines internal solitary wave theory and then reviews previous work on deep-water waves. The experiments are

described in §3, with observations and measurements of isolated and interacting waves presented in §§4 and 5 respectively. Section 6 summarizes the results and details several unresolved issues.

2. Review of the literature

It is convenient to classify internal solitary waves as 'shallow-water' waves, 'deep-water' waves or 'finite-depth' waves depending on the relative magnitudes of the total fluid depth, the depth of the stratification and the wavelength. These classes of waves are briefly discussed and then a detailed review of deep-water waves is presented.

2.1. *Overview of internal solitary wave theory*

Theoretical work on internal solitary waves was initiated by Keulegan (1953) and Long (1956), who showed that such waves can propagate on the interface between two fluids of different densities. Following this, Benney (1966) and Benjamin (1966) derived the evolution equation governing solitary waves of small-but-finite amplitudes, with wavelengths much greater than the total fluid depth, propagating in continuously stratified fluids where the depth of the stratification is similar to the total fluid depth. These waves are called shallow-water waves, for which the principal assumptions are

$$\lambda/H \gg 1 \quad \text{and} \quad h/H = O(1), \tag{2.1}$$

where $2H$ is the total fluid depth and $2h$ is the depth of the stratification. For a balance between dispersion and nonlinearity the wavelength–amplitude scaling is

$$(\lambda/H)^2 = O(a/H)^{-1}, \tag{2.2}$$

where a is the amplitude.

The extension of shallow-water theory to account for waves propagating on a thin pycnocline in an unbounded fluid was presented by Benjamin (1967) and Davis & Acrivos (1967). These waves are called deep-water waves and have wavelengths which are much smaller than the total fluid depth but much greater than the depth of the stratification:

$$\lambda/H \to 0 \quad \text{and} \quad \lambda/h \gg 1. \tag{2.3}$$

For a balance between dispersion and nonlinearity the wavelength–amplitude scaling is

$$\lambda/h = O(a/h)^{-1}. \tag{2.4}$$

Joseph (1977) and Kubota, Ko & Dobbs (1978) extended the shallow- and deep-water theories to account for waves of small-but-finite amplitudes propagating in fluids which are neither shallow nor deep, but in which the total fluid depth is much greater than the depth of the stratification. These waves are called finite-depth waves and have wavelengths which are much greater than the depth of the stratification:

$$h/H \ll 1 \quad \text{and} \quad \lambda/h \gg 1. \tag{2.5}$$

Differences between these classes of waves are due to differences in dispersion. The phase speeds of long shallow- and deep-water waves are $c_0(1-\beta k^2)$ and $c_0(1-\gamma\,|\,k\,|)$ respectively, where γ is a positive constant. Comparing these expressions indicates that for shallow- and deep-water waves with identical $\lambda/H, \lambda/h$ ratios the deep-water waves must be more nonlinear in order to propagate with permanent form. In turn,

finite-depth waves have phase speeds with a transcendental wavenumber dependence,

$$c = c_0 \left[1 - \frac{1}{2}kh\left(\coth(kH) + \frac{1}{kH}\right)\right], \tag{2.6}$$

that reduces to the shallow-water relation in the limit $kH \ll 1$ (i.e. $k\coth(kH) \to k^2$) and the deep-water relation in the limit $kH \to \infty$ (i.e. $k\coth(kH) \to |\, k\,|$).

2.2. *Deep-water internal solitary waves*

In contrast to the vast number of studies of shallow-water waves, there have been few studies of deep-water waves. Theoretical studies have focused on the mathematically amenable problem of steady waves of small-but-finite amplitudes propagating in weakly stratified inviscid fluids. As computational power has increased, time-dependent, arbitrary amplitude and dissipative flows have been investigated numerically. However, to illustrate the principal theoretical results, it is sufficient to consider steady waves.

Dubreil-Jacotin (1937) and Long (1953) showed that steady two-dimensional motions of an incompressible inviscid stratified fluid are governed by the conservation of vorticity equation

$$\nabla^2\psi + \frac{1}{\rho}\frac{\partial\rho}{\partial\psi}\left[\tfrac{1}{2}\left(\psi_x^2 + \psi_z^2\right) + gz\right] = \mathscr{H}_\infty(\psi), \tag{2.7}$$

where (x, z) are the horizontal and vertical coordinates, $\nabla^2 = \partial^2/\partial x^2 + \partial^2/\partial z^2$ is the Laplacian operator, $\psi(x, z)$ is the two-dimensional streamfunction, $\rho(x, z)$ is the fluid density, g is the gravitational acceleration and $\mathscr{H}_\infty(\psi)$ is a function determined by the upstream conditions. This equation can be used to consider the steady motions associated with a wave propagating at constant velocity c through a stationary environment by employing a coordinate system which moves with the wave. In this reference frame there is a uniform flow upstream and thus

$$\mathscr{H}_\infty(\psi) = \frac{1}{\rho}\frac{\partial\rho}{\partial\psi}\left(\frac{c^2}{2} + \frac{g\psi}{c}\right). \tag{2.8}$$

To simplify the analysis the following non-dimensional variables are introduced:

$$\tilde{x} = x/h, \quad \tilde{z} = z/h \quad \text{and} \quad \tilde{\psi} = \psi/(ch), \tag{2.9}$$

and the stratification expressed as

$$\rho(\psi) = \bar{\rho}[1 - \sigma\mathscr{F}(\tilde{\psi})], \tag{2.10}$$

where hereinafter $\overline{(\,)}$ denotes a vertically averaged quantity, σ is the non-dimensional density difference and $\mathscr{F}(\tilde{\psi})$ is an arbitrary monotonically increasing function. Furthermore, to focus on the deviations from the uniform flow, the perturbation streamfunction $\tilde{\phi}(\tilde{x}, \tilde{z})$ is used

$$\tilde{\psi} = \tilde{\phi} + \tilde{z}. \tag{2.11}$$

By substitution it can be shown that the governing equation may be rewritten as

$$\nabla^2\tilde{\phi} + \Lambda\left(\frac{\mathscr{F}_\psi}{1 - \sigma\mathscr{F}}\right)\tilde{\phi} = -\frac{1}{2}\left(\frac{\sigma\mathscr{F}_\psi}{1 - \sigma\mathscr{F}}\right)\left(\tilde{\phi}_{\tilde{x}}^2 + \tilde{\phi}_{\tilde{z}}^2 + 2\tilde{\phi}_{\tilde{z}}\right), \tag{2.12}$$

where the subscripts indicate derivatives and

$$\Lambda^{-1} \equiv c^2/\sigma gh = c^2/2c_0^2. \tag{2.13}$$

In general, the Boussinesq approximation, which neglects density variations in the inertial terms of the equations of motion, is applied and the Dubreil-Jacotin–Long equation reduces to

$$\nabla^2\tilde{\phi} + \Lambda\mathscr{F}_\psi(\tilde{\phi} + \tilde{z})\tilde{\phi} = 0. \tag{2.14}$$

This approximation must be used with caution however. For example, Long (1965) and Benjamin (1966) found weakly nonlinear shallow-water waves that are extinguished in the Boussinesq limit. In addition, for stratifications with a buoyancy frequency which is symmetric about the centre of the fluid layer, $\mathscr{F}_\psi(\psi) = \mathscr{F}_\psi(-\psi)$, applying the Boussinesq approximation restricts the analysis to antisymmetric waves, i.e. $\phi(-z) = -\phi(z)$. Despite these problems, (2.14) has been used in almost all theoretical investigations.

Although simplified, the Boussinesq form of the governing equation remains nonlinear and thus Davis & Acrivos first sought approximate analytic results for waves of small-but-finite amplitudes. Following the approach used for shallow-water waves, they expanded the streamfunction and wavespeed in powers of the amplitude

$$\tilde{\phi} = \left(\frac{a}{h}\right)\tilde{\phi}^{(1)} + \left(\frac{a}{h}\right)^2\tilde{\phi}^{(2)} + \ldots \quad \text{and} \quad \Lambda = \Lambda^{(0)} + \left(\frac{a}{h}\right)\Lambda^{(1)} + \ldots, \tag{2.15}$$

and then enforced the deep-water wavelength–amplitude scaling (2.4) by setting the x-derivatives to be $O(a/h)$ smaller than the y-derivatives. Ignoring terms of $O(a/h)^3$ then allowed weakly nonlinear solutions to be found for two layers of different density separated by a thin constant-gradient region and for a continuous stratification of the form

$$\rho(z) = \overline{\rho}[1 - (\Delta\rho/2\overline{\rho})\tanh(z/h)]. \tag{2.16}$$

For this latter stratification the wavespeed increased with increasing amplitude

$$c/c_0 = 1 + 0.3(a/h) + O(a/h)^2. \tag{2.17}$$

This result was independently derived by Benjamin (1967), who also showed that waves have Lorentzian profiles

$$\phi = a\lambda^2/(x^2 + \lambda^2) \tag{2.18}$$

and that for the $\tanh(z/h)$ stratification the exact wavelength–amplitude scaling is

$$\lambda = 5/2a. \tag{2.19}$$

In addition to finding the exact solution for steady waves, Benjamin derived the equation governing unsteady waves by modifying the dispersion term in the shallow-water evolution equation to that appropriate for long infinitesimal deep-water waves.

The existence of such waves was confirmed experimentally by Davis & Acrivos, who showed that they form when a small quantity of neutrally buoyant fluid is injected into a slightly diffused density interface between two deep fluids of different densities. Two types of waves are observed. First, there are 'small-amplitude' waves characterized by open streamlines, fluid particle velocities less than the wave speed and behaviour similar to that predicted by the weakly nonlinear theory. These waves propagate with only gradual amplitude attenuation, reflect off solid vertical boundaries without apparent energy loss and two such waves travelling in opposite directions pass through each other unchanged. Second, there are 'large-amplitude' waves characterized by a region of fluid trapped within closed streamlines, fluid particle velocities approximately equal to the wavespeed and behaviour qualitatively different from that of the small-amplitude waves. Subsequently, Maxworthy (1980)

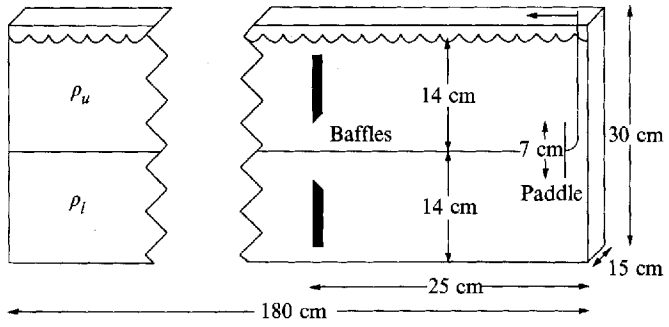

FIGURE 1. Experimental setup. Large-amplitude mode-2 waves were generated by smoothly displacing the paddle along the interface and then bringing it to rest between the two baffles.

showed that a train of large-amplitude waves can form from quite general forcing mechanisms when the appropriate environmental conditions exist. The waves are ordered according to amplitude, with the large fast waves leading the small slow waves, and the recirculating region of each wave consists of two counter-rotating cells.

To extend their approximate analytic results, Davis & Acrivos computed numerical solutions for waves on a thin constant-gradient region separating two deep layers of different densities and found that for amplitudes $a/h > 1.2$ the central streamline bifurcates, trapping fluid within closed streamlines. Although the flow field and wavespeeds computed for these waves were consistent with those of experiments, the analysis was invalidated by the presence of streamlines unconnected to the upstream flow. Furthermore, the usefulness of inviscid solutions is questionable because the diffusion of vorticity plays an important role in the dynamics of flows within closed streamline regions (Batchelor 1956). However, Tung *et al.* (1982) argued that such solutions are valid for times long enough that transient behaviour is negligible but short enough that viscosity is unimportant, and then computed solutions for large-amplitude waves on a $\tanh(z/h)$ stratification. Their focus was on shallow- rather than deep-water waves, although it was shown that for practical purposes the deep-water regime occurs for $H/h \geqslant 40$.

3. Description of the experiments

This investigation uses laboratory experiments to extend our understanding of deep-water waves with recirculating regions and thereby avoids the problems encountered in modelling efforts. A description of the experimental methods is presented in this section.

3.1. *Apparatus and procedure*

The experiments were carried out in a glass channel of horizontal cross-section $L \times w = 180 \times 15$ cm (figure 1). A continuously stratified fluid was formed by floating a layer of fresh water on top of a layer of salt water through two diffusers and letting the interface produced thicken by diffusion. The salt water was easily adjusted to the desired density, and the layer depths were chosen to be as large as possible, $H = 14$ cm, to ensure that the waves generated were deep-water waves. The filling procedure took about 20 minutes. Then the diffusers were removed, leaving a free upper surface, and the interface allowed to thicken for a further 10 minutes.

At the end of this time the density stratification was examined by traversing

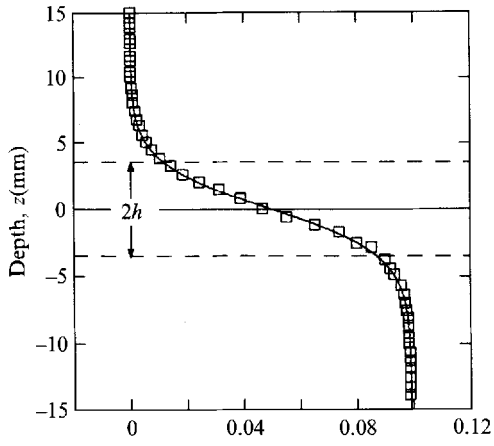

FIGURE 2. Experimental (□) and theoretical (———) density stratifications. The experimental stratification was formed by allowing the interface between fresh and salt water layers to thicken by diffusion.

a four-wire conductivity probe (Precision Measurement Engineering, USA, Model MSCI-PME 106-300E) and fast-response glass thermistor (Fenwal Electronics, USA, Model 0.070 inch diameter) through the interface. The measured conductivities were normalized to 20 °C by assuming a 2.25% change per degree Celsius, and Weast's (1975) data used to calculate the densities at 20 °C. In all experiments the measured stratifications were well described by the $\tanh(z/h)$ profile used in theoretical work, with a characteristic depth of about 2.5 mm (figure 2). Thus the ratio of the total fluid depth to the depth of the stratification was about $H/h = 50$, which is within the deep-water regime (Tung *et al.*).

For a more accurate measure of the density difference across the interface, samples were withdrawn from the centre of both layers and their density at 20.00 ± 0.01 °C measured to $\pm 7 \times 10^{-5}$ gm cm^{-3} using a digital densimeter (Anton Paar, K. G. Austria, Model DMA 02C).

The setup used to generate large-amplitude mode-2 waves (lowest-order varicose mode) is shown in figure 1. A paddle of depth 7 cm, which extended across the channel and was centred on the interface, was smoothly displaced along the interface. Interfacial fluid became trapped against the moving paddle and when the paddle was brought to rest between two polystyrene baffles this fluid slumped into the main chamber of the channel forming a large-amplitude solitary wave. The baffles prevented the intermediate-density fluid created by mixing behind the paddle from entering the main chamber of the channel and interacting with the wave. However, in response to the injection of fluid into the main chamber of the channel, fluid flowed over the upper baffle and back into the generation chamber until both chambers equilibrated to equal depths. This generation technique was used because it consistently produced a single large-amplitude wave rather than several amplitude-ordered waves. Furthermore, the position and number of paddles was easily changed thereby allowing wave–boundary and wave–wave interactions to be simply set up.

3.2. *Flow visualization*

Several flow visualization techniques were employed and all experiments were recorded on video for subsequent analysis.

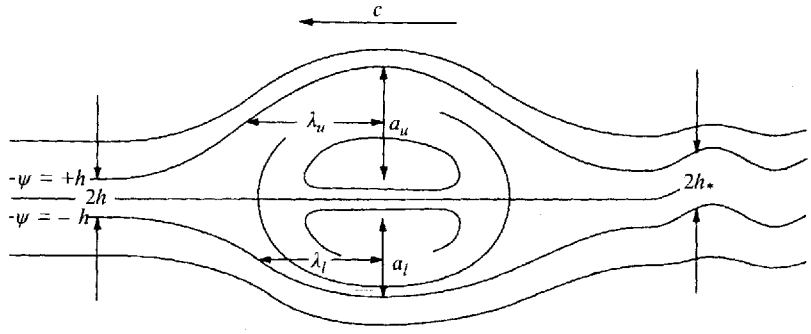

FIGURE 3. Definitions of amplitude (a) and wavelength (λ) for mode-2 waves. The amplitude was defined as the maximum displacement of the $\psi = \pm h$ streamlines and the wavelength as the forward half-width at half-maximum of these streamlines. Note that the thickness of the interface behind the wave ($2h_*$) was larger than that ahead of the wave ($2h$) due to the wave-induced mixing.

To determine the position, amplitude and wavelength of the waves, coloured water-insoluble droplets of different densities were injected into the fluid. Spread out along the channel, these droplets marked surfaces of constant density and thus the streamlines of the flow (figure 4). Mixtures were made to within ± 0.0005 gm cm^{-3} of the desired densities from heptane ($\rho = 0.6840$ gm cm^{-3} at 20 °C), 1-bromopentane ($\rho = 1.2237$ gm cm^{-3} at 20 °C) and Sudan 3 dye. These chemicals were chosen for their insolubility in water, suitable densities and relative non-toxicity. Injecting the mixtures into the fluid with a fine-gauge hypodermic needle placed below the free surface then produced droplets of < 0.25 mm diameter. In all experiments the surfaces of constant density corresponding to $z = \pm h$ in the $\tanh(z/h)$ profile were marked to allow the depth of the stratification and, as discussed in §3.3, the wave properties to be measured.

Qualitative observations of the motion within the recirculating region of large-amplitude waves were made by injecting dye, mixed with salt water so as to be neutrally buoyant, into the centre of the interface (figure 5*a*). The dyed fluid had similar properties to the undyed fluid and was usually placed between the paddle and baffles so as to be entrained while the wave formed. In some experiments however, dye was placed in the main chamber of the channel to investigate entrainment into a fully formed wave and the centre of the interface was also marked with droplets.

3.3. *Definition and measurement of wave properties*

Measurements of amplitude and wavelength were made in accordance with the definitions employed in weakly nonlinear theory (Benjamin 1967; Davis & Acrivos 1967). Figure 3 illustrates these definitions and the general nature of the large-amplitude waves.

The amplitude was defined as the maximum displacement of the $\psi = \pm h$ streamlines

$$a = |\, \psi(\pm h) \,|_{max} - h, \tag{3.1}$$

and was measured using dyed water-insoluble droplets which were neutrally buoyant at $z = \pm h$.

The wavelength was defined as the half-width at the height where the amplitude, as defined by the $\psi = \pm h$ streamlines, was half its maximum value. However, the large-amplitude waves generated in the laboratory were followed by a mode-1 (oscillatory) wave and mixed the density stratification, and therefore did not exhibit the fore-aft

Symbol	ρ_l	ν_l/ν_u	σ	h	h_*	$\bar{a}_{max}/h$	$-\mathrm{d}\bar{a}/\mathrm{d}X$	Re_h	Re_w
△	1.0501	1.05	0.0253	2.25	3.00	3.1	0.0037	36.2	2416
□	1.1099	1.20	0.0485	2.75	3.25	2.5	0.0031	65.4	3567
○	1.1500	1.40	0.0707	2.50	2.90	3.1	0.0029	65.5	3931
×	1.1997	1.65	0.0917	2.50	3.00	2.9	0.0025	70.7	4243

TABLE 1. Experimental parameters and results for isolated waves. The list includes: the lower-layer density (ρ_l; gm cm^{-3}), the ratio of layer viscosities (ν_l/ν_u), the non-dimensional density difference (σ), the characteristic depth of the interface before (h; mm) and after (h_*; mm) the passage of the wave, the maximum non-dimensional amplitude (a_{max}/h), the rate of amplitude attenuation ($-\mathrm{d}\bar{a}/\mathrm{d}X$), and the Reynolds numbers characterizing viscous dissipation within the interface (Re_h) and at the sidewalls (Re_w). In each experiment the layer depths were both $H = 14$ cm and the density of the fresh upper layer was $\rho_u = 0.9982$ gm cm^{-3}.

symmetry of theoretical profiles. Thus wavelength measurements were restricted to the forward portion of the wave and the depth of the undisturbed interface ahead of the wave used for non-dimensionalizations.

Measurements of time, amplitude and wavelength were made every 5 cm. The wave position was defined as the position of maximum displacement of the $\psi = \pm h$ streamlines, that is, the position of maximum amplitude. To account for asymmetry about the centre of the interface both the upper and lower values of the amplitude and wavelength were measured.

4. Propagation of isolated waves

A number of preliminary experiments were carried out for familiarization with the wave generation technique and wave properties. Once the experimental procedure was refined, detailed observations and measurements were made of four isolated waves for which the lower-layer densities were $\rho_l = 1.0501$, 1.1099, 1.1500 and 1.1997 gm cm^{-3} (table 1). Here the experimental results are presented and compared with theoretical predictions.

4.1. *Wave generation*

Isolated large-amplitude mode-2 waves were easily generated using the paddle technique described in §3.1. As the paddle moved along the interface the interfacial fluid was displaced from its level of neutral buoyancy and, while most fluid was deflected above and below the paddle, some fluid became trapped against the paddle. When the paddle was brought to rest this trapped fluid slumped away under the restoring force of gravity and momentum imparted by the paddle. Figure 4 shows the subsequent behaviour. The front of the intrusion took the form of a stable solitary wave while at the rear of the intrusion fluid was ejected backwards through wave-breaking. In this manner, the intrusion quickly attained a distinct length and an isolated solitary wave emerged about 20 cm from the point at which the paddle was stopped. The fluid which was not incorporated into the wave formed a gravity current intrusion and was rapidly left behind.

The largest waves were generated with an intermediate paddle speed, long paddle stroke and paddle which was deep compared to the characteristic depth of the interface. An appropriate paddle speed was determined by trial and error: at large speeds most of the fluid was deflected around the paddle, whereas at small speeds the trapped fluid collapsed away from the moving paddle. To allow for measurements

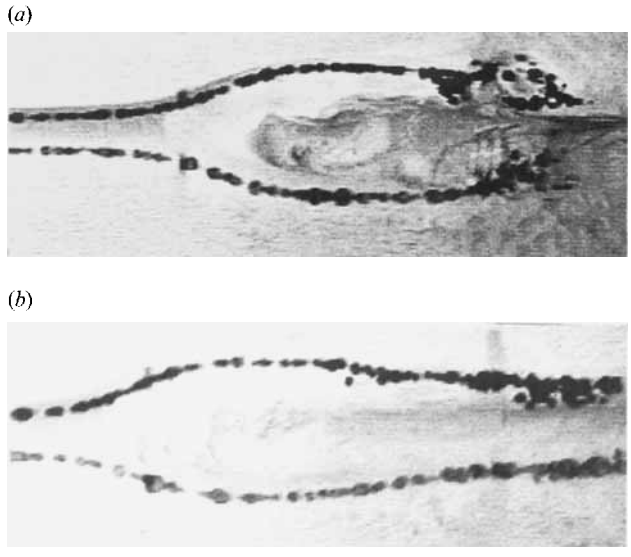

FIGURE 4. Wave generation as visualized with dyed water-insoluble droplets marking surfaces of constant density. The paddle injected fluid into the interface which (*a*) initially formed an intrusion with wave-breaking at the rear, but (*b*) seconds later the front of the intrusion had the form of a solitary wave.

over the largest possible distance, the paddle stroke was chosen to be as short as possible, 25 cm, while still ensuring that the volume of trapped fluid was large. The paddle used was as large as possible, 7 cm deep, without being so large that the volume of fluid injected into the main chamber of the channel caused a disruptive return flow over the baffles. With this setup the initial dimensional amplitude of waves was consistently about 7.5 mm for interfaces of characteristic depths $2 \leqslant h \leqslant 5$ mm. Thus the non-dimensional amplitude of waves was principally determined by the depth of the interface, and the observed maximum amplitude ($\bar{a}/h = 3.75$) was an artefact of the generation technique and interface characteristics, rather than an inherent property of the waves.†

4.2. *Experimental observations*

All waves decayed while propagating along the channel, and for large-amplitude waves this process was accompanied by a decrease in the size of the recirculating region. In general, the waves traversed the channel twice before becoming too small to trap fluid and then continued back-and-forth several more times before becoming too small to observe. Figure 5 shows the same wave at large and small amplitudes.

The large-amplitude waves had both laminar and turbulent regions: along the open streamlines the flow was laminar and fluid stratified, whereas within the closed streamline region the flow was turbulent and the fluid well-mixed. As observed in numerical solutions, the recirculating region consisted of upper and lower counter-rotating cells; however, there was no clear boundary separating the cells, and fluid was

† Motivated by this study, Matthew Stocks (private communication) carried out additional experiments with the described apparatus and generated waves of amplitude $\bar{a}/h = 5$ by further reducing the depth of the interface. Similarly large waves were also generated on a thicker interface using a convergent channel.

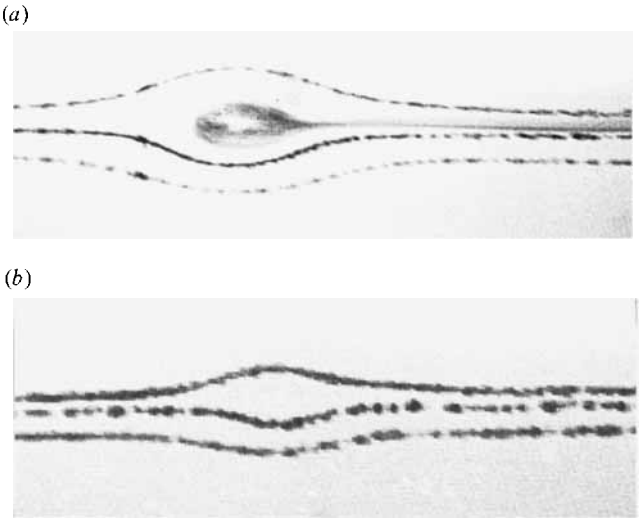

FIGURE 5. The same wave as in figure 4 at (*a*) large and (*b*) small amplitudes. In both frames the wave is propagating to the left, and the upper droplets ($\psi = h$ streamline) are displaced further than the lower droplets ($\psi = -h$ streamline). The wave passed through a region of dyed interface and in (*a*) entrained dye marks the trapped fluid. As energy was dissipated, the wave amplitude decreased, fluid was ejected from the recirculating region leaving a line of dye behind the wave, and eventually the wave became too small to trap fluid (*b*).

continuously entrained into and ejected from this region.† For example, when a wave passed through a region of dyed interface the dye mixed into the cells within several seconds only to be gradually ejected from the rear of the wave. The entrainment appeared to occur at the same rate at all points along the boundary enclosing the trapped fluid, and the rapid spread of dye through the cells was indicative of turbulent mixing. Furthermore, the rear of the wave was susceptible to shear instabilities, with smaller droplets occasionally being entrained there and carried for 10–100 cm before being ejected in a turbulent manner. Through this process of entraining, mixing and ejecting fluid the large-amplitude waves promoted localized mixing which increased the thickness of the interface, i.e. $h_* > h$ (table 1).

A mode-1 wave closely followed each mode-2 solitary wave (figures 3 and 13). The amplitude of these waves was decreased by aligning the paddle with the centre of the interface and limiting the paddle speed, but they could not be eliminated. For the most carefully controlled experiments, the mode-1 waves had amplitudes of 1–5 mm, wavelengths of 1–5 cm and appeared to propagate with permanent form. This behaviour is consistent with the prediction of Akylas & Grimshaw (1992) that internal solitary waves of mode $n > 1$ develop oscillatory tails. However, it remains possible that the waves were an artefact of the generation technique or a manifestation of shear instabilities resulting from the ejection of fluid from the main wave.

As seen in figure 5, both small- and large-amplitude waves were asymmetric about the centre of the interface, i.e. $\phi(-z) \neq -\phi(z)$. Furthermore, the upper portion of the wave was occasionally slightly ahead of or behind the lower portion of the wave. Subsequent analysis indicates that in each experiment the upper amplitude, $a_u = |\psi(+h)|_{max} - h$, was consistently greater than the lower amplitude,

† It is therefore more correct to describe the boundary of the recirculating region as an 'intermittency surface' (Townsend 1976) rather than a 'closed streamline'; however, given the historical precedent, such a change would be confusing and is avoided.

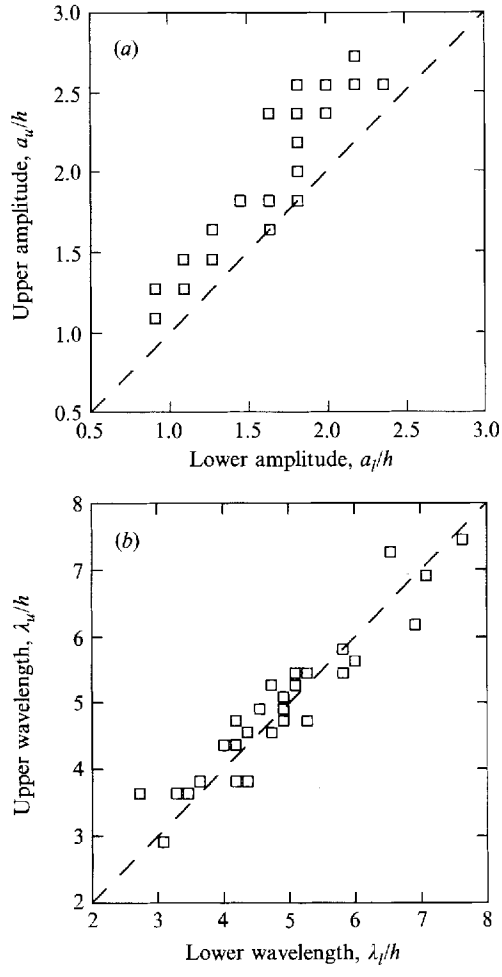

FIGURE 6. Measurements of the upper and lower values of the (*a*) amplitude and (*b*) wavelength as a wave traversed the channel. The dashed lines denote values for an antisymmetric wave, i.e. $a_u = a_l$ and $\lambda_u = \lambda_l$. In all experiments the upper amplitude was statistically greater than the lower amplitude, whereas the wavelengths were similar.

$a_l = \mid \psi(-h) \mid_{max} - h$, whereas the wavelengths were similar (figure 6). This asymmetry could have resulted from non-Boussinesq effects, the salty lower layer being more viscous than the fresh upper layer (table 1), or having a free upper but fixed lower boundary. Indeed, the Dubreil-Jacotin–Long equation indicates that for density stratifications with a symmetric buoyancy frequency, such as the $\tanh(z/h)$ stratification, Boussinesq fluids support antisymmetric waves, whereas non-Boussinesq fluids support asymmetric waves. However, experiments with different stratifications did not exhibit different wave profiles, and therefore non-Boussinesq or viscous effects do not appear to be the likely cause. Thus our preferred explanation is that the asymmetry was primarily due to the differing upper and lower boundary conditions. Whatever the case, the observed waves are similar to mode-1 waves on a slippery boundary layer waveguide, and the average amplitude, $\overline{a}$, and wavelength, $\overline{\lambda}$, values are employed in presenting further results.

Finally, all motions were two-dimensional. The waves were aligned straight across

the channel, the sidewall boundary layers were too thin to observe and there were no noticeable motions along the wave-front.

4.3. *Wavelength–amplitude scaling*

Solitary waves are characterized in terms of their wavelength–amplitude scaling, and this relationship provides a simple accurate basis for comparing experimental results with theoretical predictions.

In the experiments each wave was observed to first decrease in amplitude and wavelength while propagating along the channel; however, at some point the amplitude attenuation became accompanied by an increase in the wavelength. Thus the scaling of small and large waves was qualitatively different: at small amplitudes the wavelength decreased with increasing amplitude as predicted by weakly nonlinear theory, whereas at large amplitudes the wavelength increased with increasing amplitude.

Measurements of wavelength and amplitude were made throughout each experiment to complement the experimental observations. However, measurement errors gave rise to poorly constrained wavelength estimates for small waves, and thus it was not possible to determine the functional form of the wavelength–amplitude scaling at small amplitudes.

The wavelength and amplitude values are plotted in figure 7, and indicate that at large amplitudes the wavelength increased linearly with increasing amplitude

$$\bar{\lambda}/h = 0.95 + 2.1\bar{a}/h \quad \text{for} \quad 1.0 \leqslant \bar{a}/h \leqslant 3.1. \tag{4.1}$$

A value inferred from the $H/h = 40$ streamfunction plots of Tung *et al.* is consistent with the measurements, and this suggests that the wave behaviour can be accounted for by higher-order amplitude terms without regard to viscous effects. Indeed, at large amplitudes the important dynamical balance must be between nonlinearity and dispersion, and thus viscosity may be important in dissipating energy but should not directly affect the wave scaling.

An important outcome of this linear wavelength–amplitude relationship is that all waves of amplitudes $a/h \geqslant 1$ are similar in shape and differ only by a scaling factor. This 'self-scaling' behaviour was also reported by Pullin & Grimshaw (1988) in their numerical investigation of solitary waves on an interface between two unbounded Boussinesq fluids; indeed, in this case the limiting wave scales as $\lambda \to 2.18a$ which is remarkably similar to that observed here. The reason for this behaviour remains unclear however, although the fact that the wave steepness, a/λ, is constant and that the limiting two-fluid profile meets the interface at the Stokes angle of 120° suggests that it is related to wave stability. Whatever its origin, the self-scaling provides a basis for seeking analytical solutions and implies that the properties of all large-amplitude waves can be derived from a single numerical solution.

4.4. *Wavespeed*

Another important property of the waves is their speed of propagation. For each experiment the wavespeeds were calculated by taking the derivative of the third-degree polynomial that best fits the displacement–time measurements, i.e. $\mathrm{d}X(t)/\mathrm{d}t$ where $X(t) = A_0 + A_1 t + A_2 t^2 + A_3 t^3$. This procedure has two advantages over difference estimates, i.e. $\Delta X/\Delta t$. First, the video unit only recorded time to ± 0.1 and the curve fit smoothes the errors resulting from these quantized time measurements. Second, the derivation of an analytic expression for the wavespeed allows values to be conveniently calculated at positions where the amplitude is known. The two wavespeed estimates agree within expected uncertainties (figure 8*a*).

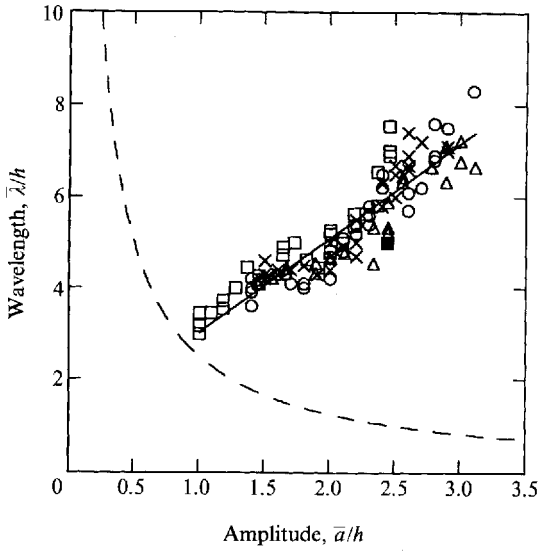

FIGURE 7. Wavelength *vs.* amplitude. In addition to the measured values, the inverse relationship derived by Benjamin using weakly nonlinear theory (– – –) and a value inferred from the $H/h = 40$ streamfunction computed by Tung *et al.* (■) are plotted. At large amplitudes the wavelength increased linearly with increasing amplitude, with the solid line being the best linear fit.

In most studies wavespeed results have been expressed in terms of the eigenvalue of the Dubreil-Jacotin–Long equation $\Lambda = 2c_0^2/c^2$. Although the relationship relating the wavespeed to the eigenvalue is simple, this approach has led to confusion in the interpretation of results and thus here the wavespeeds themselves are presented.

Figure 8(*b*) shows the wavespeed plotted against the amplitude, with Davis & Acrivos measurements included to extend the range of amplitudes. The wavespeed increased linearly with increasing amplitude according to

$$c/c_0 = 1.0 + 0.49\bar{a}/h \quad \text{for} \quad 0.1 \leqslant \bar{a}/h \leqslant 3.1. \tag{4.2}$$

The weakly nonlinear theory is accurate at small amplitudes, $\bar{a}/h < 0.5$; however, at large amplitudes the measurements are underestimated. In contrast, the $H/h = 40$ numerical solution presented by Tung *et al.* is in excellent agreement with measurements over the entire range of amplitudes. Finally, given the qualitatively different wavelength-amplitude scaling of small- and large-amplitude waves, these results indicate that the wavespeed is an insensitive measure of wave behaviour.

4.5. *Amplitude attenuation*

All waves decayed while propagating along the channel, and to elucidate the attenuation process the wave amplitude is plotted against position in figure 9(*a*). In each experiment the amplitude decreased linearly with position, and thus the rate of attenuation was constant

$$-\frac{\mathrm{d}(a/h)}{\mathrm{d}(X/h)} = -\frac{\mathrm{d}a}{\mathrm{d}X} = \text{constant}, \tag{4.3}$$

and calculated from the best linear fit to the measurements (table 1). The rates of attenuation are plotted in figure 9(*b*) and, despite the large errors, it is clear that attenuation was most rapid at small density differences.

A linear decrease of amplitude with position is not characteristic of most water

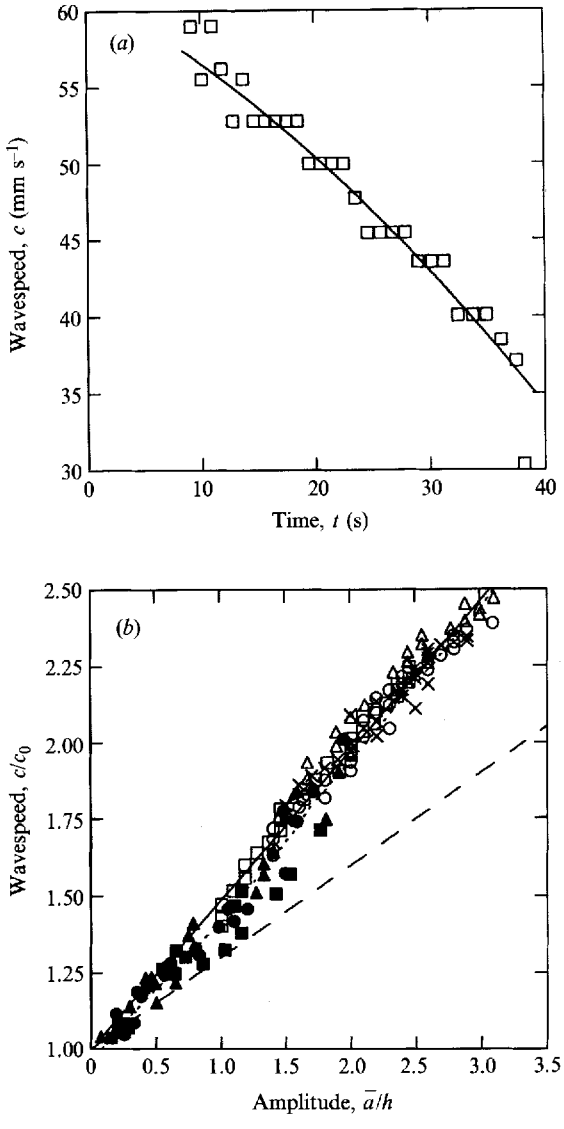

FIGURE 8. (*a*) Wavespeed estimates determined from the difference formula (□) and derivative of a polynomial fit to the displacement–time measurements (———). The polynomial fit smoothes the errors resulting from quantized time measurements. (*b*) Wavespeed *vs.* amplitude. To extend the range of amplitudes, Davis & Acrivos' measurements are included: $\rho_l = 1.052$ gm cm^{-3} (▲), $\rho_l = 1.095$ (■) and $\rho_l = 1.168$ (•). For comparison, the prediction of weakly nonlinear theory (— — —) and the $H/h = 40$ numerical solution of Tung *et al.* (· · · · · ·) are plotted. The wavespeed increased linearly with increasing amplitude, with the solid line being the best linear fit.

waves. For example, both free surface waves (Lighthill 1978) and waves on an interface between two fluids of different densities (Koop & Butler 1981) attenuate more rapidly at large amplitudes than at small amplitudes, and thus exhibit an exponential decrease of amplitude with position. It is possible that similar behaviour occurs in the present situation but was not observed because of the limited range of amplitudes considered. However, here dissipation occurred through turbulent mixing and, possibly, wave radiation as well as viscous stresses, and this difference probably

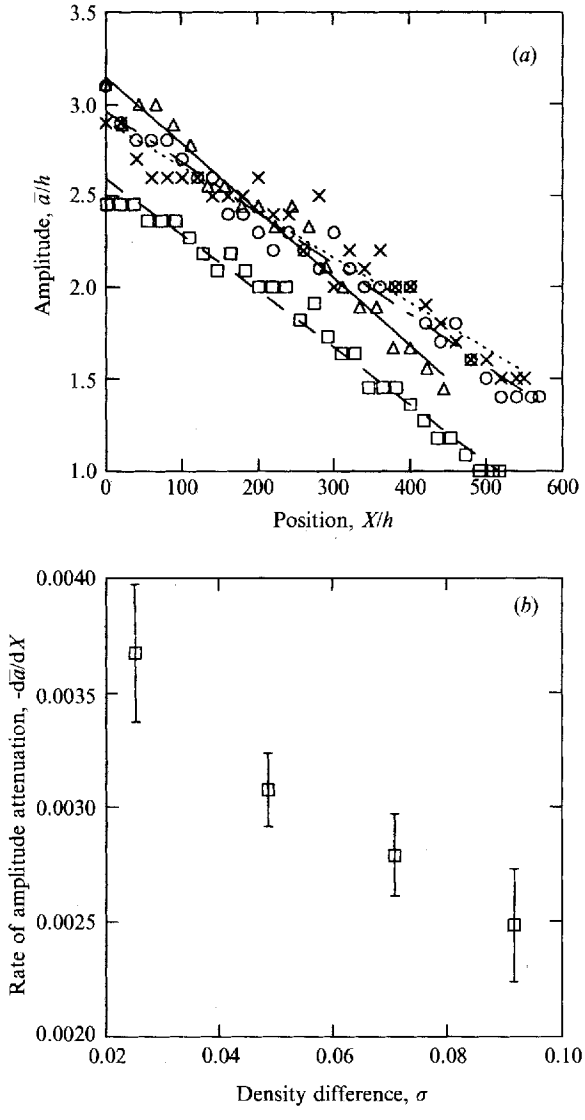

FIGURE 9. (*a*) Amplitude *vs.* position. In each experiment the amplitude decreased linearly with position, and thus the rate of attenuation ($-da/dX$) was independent of the amplitude. The best linear fit is plotted for each experiment: $\rho_l = 1.05$ (———), $\rho_l = 1.10$ (– – –), $\rho_l = 1.15$ (—— - ——) and $\rho_l = 1.20$ (·····). (*b*) Attenuation rate *vs.* density difference. Despite the large errors, it is clear that the most rapid attenuation occurred at small density differences.

accounts for the observed behaviour. An attempt is now made to determine the relative importance of these three dissipation mechanisms.

If viscous stresses were the dominant dissipation mechanism, then the rate of attenuation should depend on the Reynolds number: $Re = UL/\nu$ where U is the velocity scale, L is the length scale and ν the kinematic viscosity. Here attenuation was independent of amplitude and therefore the Reynolds numbers characterizing the flow should also be independent of amplitude. Thus an appropriate velocity scale is the speed of long infinitesimal waves, and the length scales are taken to be the

characteristic depth of the interface for dissipation within the interface

$$Re_h = c_0 h/\nu \propto (\sigma g h^3)^{1/2}/\nu(\overline{\rho}), \tag{4.4}$$

and the channel width for dissipation at the sidewalls

$$Re_w = c_0 w/\nu \propto (\sigma g h)^{1/2} w/\nu(\overline{\rho}), \tag{4.5}$$

where $\nu(\overline{\rho})$ is the average viscosity of the two layers as calculated from Weast's data. Values of the Reynolds numbers are listed in table 1. The change in the velocity scale caused by changes in the density difference dominate the associated changes in the viscosity, and thus both Reynolds numbers increase with increasing density difference. This result is consistent with the observation that the most rapid attenuation occurred at small density differences, and, as observed in the preliminary experiments, indicates that the rate of attenuation should decrease when either the characteristic depth of the interface or channel width increase.

Large-amplitude waves entrained, mixed and then ejected fluid, and thus turbulent mixing occurred both within the recirculating region as well as between this region and the surrounding flow. This mixing affected wave attenuation in two ways. First, kinetic energy was extracted from the wave and used to increase the potential energy of the water column (table 1). Second, the wave experienced drag due to the loss of high-momentum fluid from its recirculating region. Whilst it is difficult to quantify these effects, the mixing itself appeared to result from shear instabilities and should therefore depend on the Richardson number $Ri = g\Delta\rho L/\overline{\rho}(\Delta U)^2$. Again the velocity scale is taken to be the speed of long infinitesimal waves and the length scale to be the depth of the stratification. This approach produces a constant Richardson number

$$Ri \propto g\Delta\rho h/\overline{\rho}c_0^2 \equiv g\Delta\rho h/\overline{\rho}(\sigma g h) \equiv \text{constant}, \tag{4.6}$$

and thus changes in the interfacial density difference lead to changes in the stabilizing restoring force and destabilizing shear that balance. Therefore all waves should have had the same susceptibility to shear instabilities and, if turbulent mixing was the dominant dissipation mechanism, decayed at the same rate. Hence it appears that turbulent mixing cannot explain the observation that attenuation was most rapid at small density differences.

As discussed in §4.2, a mode-1 wave followed each mode-2 wave, and these waves may have carried energy away from the main wave. Akylas & Grimshaw (1992) predicted the existence of such waves but were unable to calculate the resulting attenuation of the mode-2 wave. However, a crude estimate can be made by noting that the radiation of energy in an attached infinitesimal lee wave train is equal to

$$\frac{\mathrm{d}E}{\mathrm{d}t} \propto w(c - c_g)\epsilon \tag{4.7}$$

where $c_g = \mathrm{d}(ck)/\mathrm{d}k$ is the group velocity and ϵ the energy per unit area of the attached waves (Lighthill 1978). The energy of a large-amplitude mode-2 wave might be expected to vary as

$$E \propto w\lambda(\overline{\rho}ac^2 + g\Delta\rho a^2), \tag{4.8}$$

where the first term is the kinetic energy contribution due to the bulk motion and the second term represents the potential energy and remaining kinetic energy contributions. Now, for infinitesimal waves on an interface between two unbounded fluids of different densities

$$c^2 = g\sigma/k, \quad c_g = c/2 \quad \text{and} \quad \epsilon = g\Delta\rho\xi^2/2, \tag{4.9}$$

where ξ is the wave amplitude. Substituting, using the empirical relations for wavespeed (4.2) and wavelength (4.1), and taking the limit $a/h \gg 1$ gives

$$\frac{\mathrm{d}a}{\mathrm{d}X} \propto \frac{h\xi^2}{a^3}, \tag{4.10}$$

where the chain rule has been used. Here the amplitude of the attached waves appeared to be constant, and this result therefore indicates that if wave radiation had been the dominant dissipation mechanism then the attenuation rate should depend on the amplitude itself. In practice however, the attenuation was independent of amplitude, and thus wave radiation does not appear to explain the experimental results.

In summary, evidence for a linear decrease of amplitude with position is convincing, and observations indicate that dissipation occurred through viscous stresses, turbulent mixing and, possibly, wave-radiation. Attenuation was most rapid at small density differences. This trend is consistent with Reynolds number trends, whereas neither a Richardson number formulation of the turbulent mixing nor an estimate of the radiation of energy by the mode-1 waves predicts the observed behaviour. However, the theoretical approaches used in these estimates were rather crude, and further work is required before a complete understanding of the wave attenuation is attained.

5. Wave–boundary and wave–wave interactions

Since the discovery by Zabusky & Kruskal (1965) that solitary waves are stable and emerge from nonlinear interactions unchanged there has been much interest in interactions between solitary waves. Indeed, 'solitons' are now known to occur in numerous physical systems and illustrate how coherent behaviour can form out of chaotic conditions (Krumhansl 1991).

Interactions between solitary water waves are of special interest because they are observed in various geophysical and technological settings, and are amenable to experimental as well as theoretical investigation. For example, to understand solitary Rossby waves in Jupiter's atmosphere, Maxworthy (1976) and Weidman & Maxworthy (1978) carried out experimental investigations of head-on and overtaking collisions between solitary waves on the free surface of a shallow layer of fluid.† In both cases the waves suffered a phase shift, and the maximum wave amplitude attained during head-on collisions was greater than twice that of the incident waves. This behaviour was in qualitative agreement with weakly nonlinear theory; however, more detailed subsequent investigations have questioned whether the waves strictly behave as solitons (Fenton & Rienecker, 1982; Renouard, Seabra-Santos & Temperville, 1985).

More recently, Christie (1992) reported observations of collisions between southerly and northeasterly morning glory roll clouds, and suggested that similar collisions occur elsewhere between thunderstorm-generated solitary waves. As a first step towards understanding these interactions, experiments were carried out to determine the behaviour of deep-water solitary waves during reflection from a solid vertical boundary and head-on collisions. These interactions were simpler to set up than the observed oblique interactions, and attempts to set up overtaking collisions failed because the channel was too short. (A small slow wave ahead of a large fast wave

† Some authors have followed Miles (1977) in using the adjectives 'weak' and 'strong' to distinguish the short-time interactions of head-on collisions and the long-time interactions of overtaking collisions.

X	h_i	h_r	$(\bar{a}/h)_i$	$(\bar{a}/h)_r$	$(c/c_0)_i$	$(c/c_0)_r$	$-\Delta X$	Δt
80	2.25	2.50	2.2	1.9	2.2	1.7	7	0.3
120	2.25	2.50	2.0	1.7	2.0	1.5	3	0.2
155	2.75	3.25	1.0	0.8	1.5	1.2	4	0.4

TABLE 2. Experimental parameters and results for wave-boundary interactions, where the subscripts i and r refer to the incident and reflected waves. The list includes: the distance travelled by each wave before reflection (X; cm), the characteristic depth of the interface (h; mm), the non-dimensional amplitude ($\bar{a}/h$), the non-dimensional wavespeed (c/c_0), and the spatial ($-\Delta X$; mm) and temporal (Δt; s) phase shifts. In each experiment the layer depths were both $H = 14$ cm, the density of the lower layer was $\rho_l = 1.1000$ gm cm^{-3} and the density of the fresh upper layer was $\rho_u = 0.9982$ gm cm^{-3}. (The estimates of the spatial and temporal phase shifts are left as dimensional quantities because the increase in interface thickness during the passage of the incident wave results in different length and time scales being appropriate to the incident and reflected waves.)

was generated by stopping and then restarting the paddle.) Particular attention was given to large-amplitude waves because the atmospheric waves often have amplitudes comparable to the depth of the inversion layer. This approach also complements that of Matsuno (1979), who showed that in the weakly nonlinear limit mode-1 deep-water waves emerge from overtaking collisions along their precollision trajectories.

5.1. *Reflection from a solid vertical boundary*

To investigate the behaviour of waves during reflection from a solid vertical boundary the paddle was positioned so that waves propagated $X = 80$, 120 and 155 cm before reaching the channel endwall. Amplitude attenuation then ensured that the waves had different amplitudes at the endwall, although in each case the incident wave was large enough to contain fluid at the first reflection and the behaviour at small amplitude had to be determined from subsequent reflections (table 2). In all experiments the density of the lower layer was $\rho_l = 1.1$ gm cm^{-3} and the density of the fresh upper layer was $\rho_u = 0.9982$ gm cm^{-3}.

In all cases the reflection process began with the vertical deflection of streamlines and decrease in wavespeed, and culminated with the wave coming to rest against the endwall with an amplitude about twice that of the incident wave. Then the wave collapsed away from the endwall and appeared to recover its equilibrium profile after travelling about 20 cm. There were qualitative differences between the behaviour of small- and large-amplitude waves however: at small amplitudes there was no noticeable change in the wave, whereas at large amplitudes the reflected wave was smaller, and slower, than the incident wave (table 2). This decrease in amplitude occurred because fluid was ejected from the large-amplitude waves during the collapse away from the endwall, with, as during wave generation, this fluid forming a gravity current intrusion which was rapidly left behind (figure 10). It was not possible to determine whether the behaviour was sensitive to the amplitude of the incident wave, but the $X = 155$ cm wave suffered a much larger decrease in amplitude than the other waves. This anomalous behaviour probably occurred because on reaching the endwall this wave was only just large enough to contain fluid and it ejected all of this fluid during the reflection.

Figure 11(*a*) shows the trajectory followed by the $X = 80$ cm wave during reflection. As indicated, extrapolating lines fitted to the incident and reflected trajectories suggests that the wave suffered a small negative spatial phase shift, that is, appeared to reflect from a virtual endwall behind the real endwall or, alternatively, hesitate at the endwall.

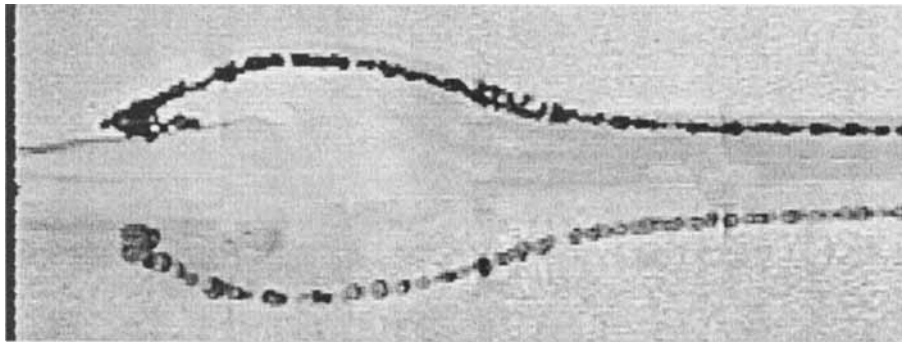

FIGURE 10. The $X = 80$ cm wave breaking and ejecting fluid as it reflects from the endwall.

Estimates of the spatial ($-\Delta X$) and temporal (Δt) phase shifts are listed in table 2, and figure 11(*b*) shows the spatial phase shift plotted against wave amplitude. A number of difficulties were encountered in deriving these estimates: the presence of the trailing oscillatory disturbance and the mixing of the density stratification by the incident wave both affected the reflected wave, and measurements had to be made far enough from the endwall to ensure that the wave was in equilibrium yet close enough to avoid significant amplitude attenuation. Nevertheless, evidence for phase shifts is convincing, with a statistical average of point estimates giving a non-zero value in the same direction as that suffered by solitary waves on the free surface of a shallow layer of fluid (Renouard *et al.* 1985).

5.2. *Head-on collision between two waves*

Several experiments were conducted to investigate the behaviour during head-on collisions between two waves propagating in opposite directions. Collisions between waves of equal amplitude were set up by displacing two paddles at the same time, whereas collisions between waves of different amplitudes were set up by displacing two paddles at different times. The distance that the waves propagated before colliding was varied but the channel was too short for a large range of amplitudes to be examined. Another problem was that it was difficult to make detailed measurements of both waves with a single video camera. In all experiments the density of the lower layer was $\rho_l = 1.1$ gm cm^{-3} and the density of the fresh upper layer was $\rho_u = 0.9982$ gm cm^{-3}.

Figure 12 shows the collision between large-amplitude waves of equal amplitude. The behaviour was similar to a reflection from a solid vertical boundary, with the fluid trapped within each wave reversing direction and being transported away from the collision along the path by which it approached. Some fluid was ejected as the waves collapsed away from each other, causing the outgoing waves to be smaller than the ingoing waves and producing small secondary waves. After reflecting off the paddle apparatus, the two waves returned to the point of the original collision which, in agreement with the direct measurements, indicates that both outgoing waves had the same amplitude.

As shown in figure 13, for waves of different amplitudes this behaviour was modified by the exchange of fluid from the larger incident wave to the smaller incident wave such that the leftward and rightward propagating waves had the same amplitudes before and after the collision. This transfer of fluid was required to satisfy conservation of momentum. Furthermore, although the trapped fluid was principally

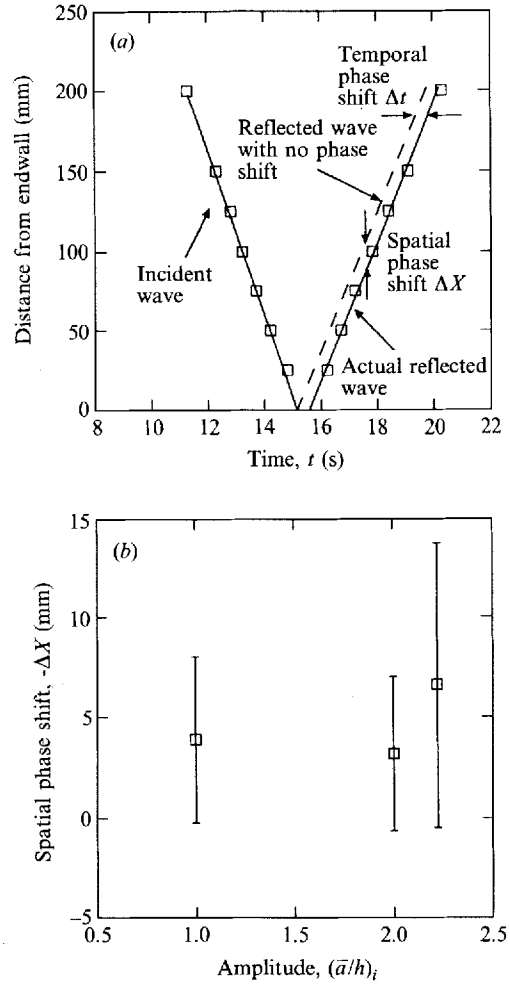

FIGURE 11. (*a*) The trajectory followed by the $X = 80$ cm wave during reflection. Extrapolating straight lines fitted to the incident and reflected trajectories indicates that the wave suffered a negative spatial phase shift. (*b*) Spatial phase shift *vs.* incident wave amplitude. The estimation procedure produces large errors, but evidence for phase shifts is convincing with the point estimates indicating that all waves suffered similar delays.

reflected during head-on collisions, the waves themselves behaved like solitons in preserving their identity while they passed through each other.

6. Summary and conclusions

An investigation of deep-water internal solitary waves has been presented. Small waves carried energy and momentum, whereas sufficiently large waves also entrained, mixed and then ejected fluid. The small-amplitude waves are well described by inviscid weakly nonlinear theory (Benjamin 1967; Davis & Acrivos 1967) but, as expected, the theory fails to predict the behaviour of the large-amplitude waves. However, numerical solutions for inviscid waves (Tung *et al.* 1982) are consistent with the observed behaviour of large-amplitude waves, and, with these solutions being invalid for flows having closed streamlines, this implies that such waves can be

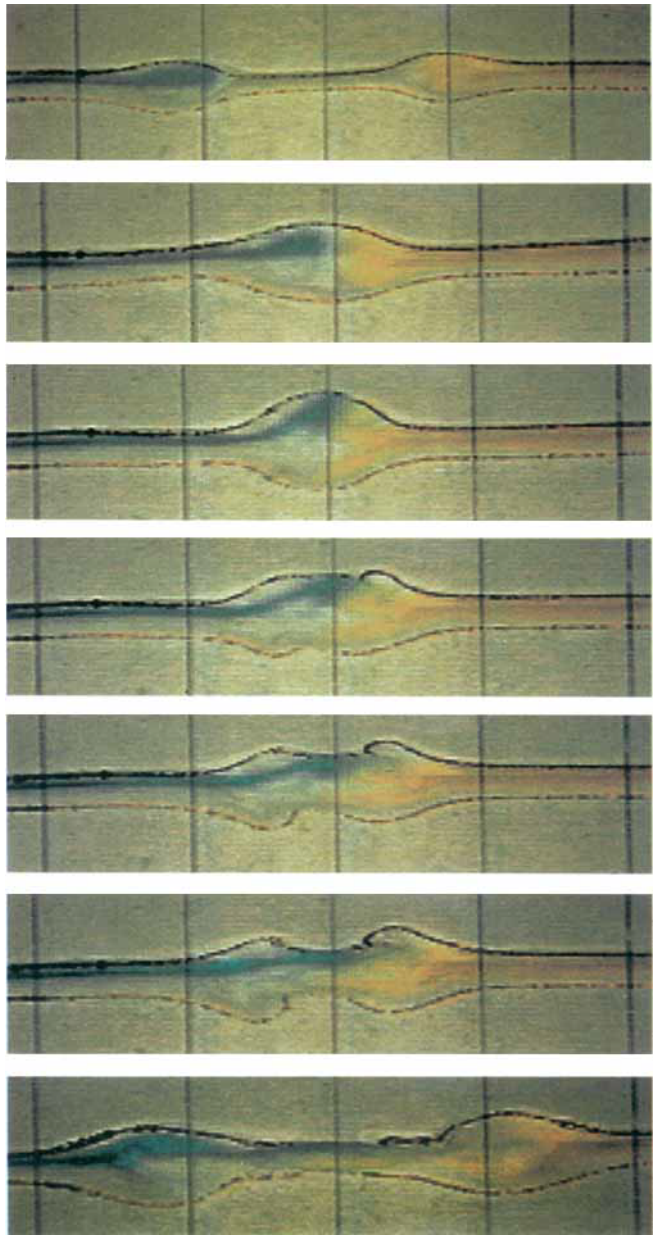

FIGURE 12. Head-on collision between two waves of equal amplitudes. The behaviour was similar to a reflection, with the fluid trapped within each wave reversing direction and being transported away from the collision along the path by which it approached.

accounted for without regard to the detailed nature of the trapped flow and viscous effects.

Several avenues for future work exist. First, a numerical investigation is required to determine if there is a critical amplitude above which waves are unstable. Indeed, whilst the finding that wave steepness is constant at large amplitudes suggests that waves of unbounded amplitude may exist, very large waves might be susceptible to

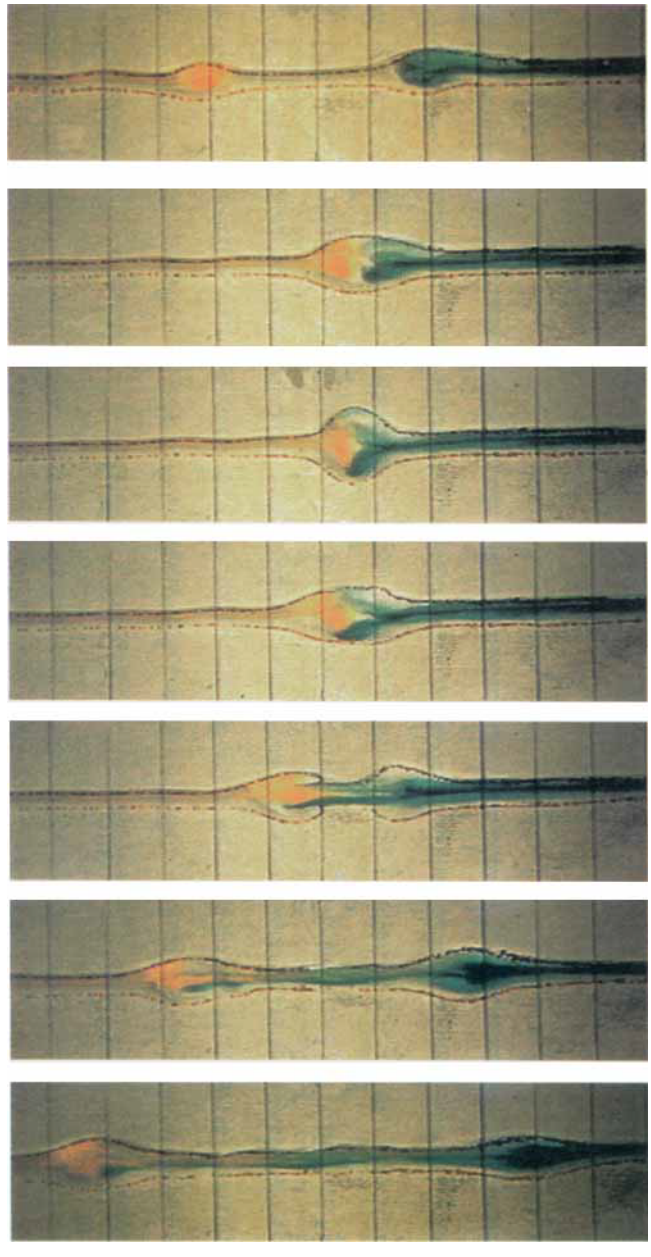

FIGURE 13. Head-on collision between two waves of different amplitudes. Whilst most of the trapped fluid was reflected, a small quantity of fluid was exchanged from the larger incident wave to the smaller ingoing wave such that the leftward and rightward propagating waves had the same amplitudes before and after the collision.

shear instabilities or bifurcate to another, perhaps asymmetric, state. Second, the origin and influence of the mode-1 waves that followed each mode-2 wave remains to be determined after a crude comparison of the measured attenuation of the main wave with that expected from wave radiation failed to resolve the issue. Third, the role of turbulent mixing and wave radiation in the damping of large-amplitude waves deserves further experimental and theoretical consideration. Fourth, an analytical

model of the large-amplitude waves awaits development, and the relationship of these waves to vortex pairs should be clarified. Although these waves are a highly nonlinear phenomenon, the finding that both their wavespeed and wavelength increase linearly with increasing amplitude suggests an underlying simplicity, and provides a starting point for such an investigation. Finally, the observation that large-amplitude waves suffer a backward shift during interactions requires experimental and theoretical verification.

To conclude, the authors hope that this investigation will provide a basis on which to interpret field observations of deep-water waves. Indeed, Clarke, Smith & Reid's (1981) finding that weakly nonlinear theory predicts the wavespeed but underestimates the wavelength of morning glory roll clouds is explained by the observation that once waves develop a recirculating region their wavelength increases, rather than decreases, with increasing amplitude. However, the wave attenuation results should be applied with caution because common dissipation mechanisms such as vertical wave radiation were not present in the experiments.

This work was done while A.P.S. was a PhD student and M.J. a vacation scholar in the Geophysical Fluid Dynamics Group, Research School of Earth Sciences, The Australian National University. The manuscript was prepared while A.P.S. was at the School of Oceanography, University of Washington supported by the UCAR Visiting Scientist Program. The authors thank Drs Ross Griffiths and Doug Christie for many helpful comments during the preparation of this paper, and Matthew Stocks for making his experimental results available. We also appreciate the technical assistance provided by Derek Corrigan and Ross Wylde-Browne. Two anonymous referees assisted in the interpretation of the amplitude attenuation results.

REFERENCES

AKYLAS, T. R. & GRIMSHAW, R. H. J. 1992 Solitary internal waves with oscillatory tails. *J. Fluid Mech.* **242**, 279–298.

BATCHELOR, G. K. 1956 On steady laminar flow with closed streamlines at large Reynolds number. *J. Fluid Mech.* **1**, 177–190.

BENJAMIN, T. B. 1966 Internal waves of finite amplitude and permanent form. *J. Fluid Mech.* **25**, 241–270.

BENJAMIN, T. B. 1967 Internal waves of permanent form in fluids of great depth. *J. Fluid Mech.* **29**, 559–592.

BENNEY, D. J. 1966 Long nonlinear waves in fluid flows. *J. Math. Phys.* **45**, 52–63.

CHRISTIE, D. K., MUIRHEAD, K. J. & HALES, A. L. 1978 On solitary waves in the atmosphere. *J. Atmos. Sci.* **35**, 805–825.

CHRISTIE, D. R. 1992 The morning glory of the Gulf of Carpentaria: a paradigm for non-linear waves in the lower atmosphere. *Austral. Met. Mag.* **41**, 21–60.

CLARKE, R. H., SMITH, R. K. & REID, D. G. 1981 The morning glory of the Gulf of Carpentaria: An atmospheric undular bore. *Mon. Weather Rev.* **109**, 1726–1750.

DAVIS, R. E. & ACRIVOS, A. 1967 Solitary internal waves in deep water. *J. Fluid Mech.* **29**, 593–607.

DUBREIL-JACOTIN, M. L. 1937 Sur les théorèms d'existence relatifs aux ondes permanentes périodiques à deux dimensions dans les liquides hétérogènes. *J. Math. Pures Appl.* **16**, 43–67.

FARMER, D. M. & SMITH, J. D. 1980 Tidal interaction of stratified flow with a sill in Knight Inlet. *Deep-Sea Res.* **27**, 239–254.

FENTON, J. D. & RIENECKER, M. M. 1982 A Fourier method for solving nonlinear water-wave problems: application to solitary-wave interactions. *J. Fluid Mech.* **118**, 411–443.

JOSEPH, R. I. 1977 Solitary waves in a finite depth fluid. *J. Phys.* A: *Math. Gen.* **10**, L225.

KEULEGAN, G. H. 1953 Characteristics of internal solitary waves. *J. Res. Natl Bur. Stand.* **51**, 133–140.

KOOP, C. G. & BUTLER, G. 1981 An investigation of internal solitary waves in a two-fluid system. *J. Fluid Mech.* **112**, 225–251.

KRUMHANSL, J. A. 1991 Unity in the science of physics. *Physics Today* March, 33–38.

KUBOTA, T., KO, D. R. S. & DOBBS, L. D. 1978 Propagation of weakly nonlinear internal waves in a stratified fluid of finite depth. *AIAA J. Hydronaut.* **12**, 157–165.

LIGHTHILL, M. J. 1978. *Waves in Fluids.* Cambridge University Press.

LONG, R. R. 1953 Some aspects of the flow of stratified fluids 1. A theoretical investigation. *Tellus* **5**, 42–58.

LONG, R. R. 1956 Solitary waves in one- and two-fluid systems. *Tellus* **8**, 460–471.

LONG, R. R. 1965 On the Boussinesq approximation and its role in the theory of internal waves. *Tellus* **17**, 46–52.

MATSUNO, Y. 1979 Exact multi-soliton solution of the Benjamin-Ono equation. *J. Phys. A: Math. Gen.* **12**, 619–621.

MAXWORTHY, T. 1976 Experiments on collisions between solitary waves. *J. Fluid Mech.*, **76**, 177–185.

MAXWORTHY, T. 1980 On the formation of nonlinear internal waves from the gravitational collapse of mixed regions in two and three dimensions. *J. Fluid Mech.* **96**, 47–64.

MILES, J. W. 1977 Obliquely interacting solitary waves. *J. Fluid Mech.* **79**, 157–169.

OSTROVSKY, L. A. & STEPANYANTS, Y. A. 1989 Do internal solitons exist in the ocean? *Rev. Geophys.* **27**, 293–310.

PULLIN, D. I. & GRIMSHAW, R. H. J. 1988 Large-amplitude solitary waves at the interface between two homogeneous fluids. *Phys. Fluids* **31**, 3550–3559.

RENOUARD, D. P., SEABRA-SANTOS, F. J. & TEMPERVILLE, A. M. 1985 Experimental study of the generation, damping, and reflexion of a solitary wave. *Dyn. Atmos. Oceans* **9**, 341–358.

RUSSELL, J. S. 1837 Report on waves. *Tech. Rep.* 417. British Association for the Advancement of Science.

TOWNSEND, A. A. 1976 *The Structure of Turbulent Shear Flow*, 2nd edn. Cambridge University Press.

TUNG, K.-K., CHAN, T. F. & KUBOTA, T. 1982 Large amplitude internal wave of permanent form. *Stud. Appl. Maths* **66**, 1–44.

WEAST, R. C. 1975 *CRC Handbook of Chemistry and Physics*, 56th edn. CRC Press.

WEIDMAN, P. D. & MAXWORTHY, T. 1978 Experiments on strong interactions between solitary waves. *J. Fluid. Mech.* **85**, 417–431.

ZABUSKY, N. J. & KRUSKAL, M. D. 1965 Interaction of solitons in a collisionless plasma and the recurrence of initial states. *Phys. Rev. Lett.* **15**, 240–243.